Journal of Quantitative Spectroscopy & Radiative Transfer 113 (2012) 565–574

Contents lists available at SciVerse ScienceDirect

Journal of Quantitative Spectroscopy & Radiative Transfer

journal homepage: www.elsevier.com/locate/jqsrt

The Amsterdam–Granada Light Scattering Database

O. Muñoz [a,*], F. Moreno [a], D. Guirado [a,b], D.D. Dabrowska [a], H. Volten [c], J.W. Hovenier [d]

[a] Instituto de Astrofísica de Andalucía, CSIC, Glorieta de la astronomía sn, 18008 Granada, Spain
[b] Netherlands Institute for Space Research, SRON, Sorbonnelaan 2, 3584 CA Utrecht, The Netherlands
[c] Netherlands National Institute for Public Health and the Environment, Centre for Environmental Monitoring, P.O. Box 1, NL 3720 BA Bilthoven, The Netherlands
[d] Astronomical Institute "Anton Pannekoek", University of Amsterdam, Science Park 904, 1098 XH Amsterdam, The Netherlands

ARTICLE INFO

Article history:
Received 24 November 2011
Received in revised form
23 January 2012
Accepted 23 January 2012
Available online 28 January 2012

Keywords:
Scattering matrix
Experiments
Irregular particles
Polarization

ABSTRACT

The Amsterdam Light Scattering Database proved to be a very successful way of promoting the use of the data obtained with the Amsterdam Light Scattering apparatus at optical wavelengths. Many different research groups around the world made use of the experimental data. After the closing down of the Dutch scattering apparatus, a modernized and improved descendant, the IAA Cosmic Dust Laboratory (CoDuLab), has been constructed at the Instituto de Astrofísica de Andalucía (IAA) in Granada, Spain. The first results of this instrument for water droplets and for two samples of clay particles have been published. We would now like to make these data also available to the community in digital form by introducing a new light scattering database, the Amsterdam–Granada Light Scattering Database (www.iaa.es/scattering). By combining the data from the two instruments in one database we ensure the continued availability of the old data, and we prevent fragmentation of important data over different databases. In this paper we present the Amsterdam–Granada Light Scattering Database.

1. Introduction

In the last few decades, the Amsterdam light scattering setup [1] fulfilled a unique position in producing a significant amount of experimental scattering matrices as functions of the scattering angle of samples of small irregular particles relevant for astronomy, and studies of the atmosphere, as well as coastal and inland waters of the Earth (see e.g. [2–8]). The measurements of aerosols were performed at two different wavelengths (441.6 and 632.8 nm) in the scattering angle range from 3–5° (depending on the sample) to 174°. The hydrosol measurements were done at 632.8 nm in the scattering angle range from 20° to 160°. These experimental data are a powerful tool for properly interpreting space- and ground-based observations or for testing different computational approaches devoted to obtain the scattering behavior of small irregular particles (e.g. [9–16]). In addition, the light scattering results may also be applicable in the paper and paint industry, or in the fields of chemistry and biology.

Since September 2003, the Dutch experimental data are freely available in digital form in the Amsterdam Light Scattering Database [17,18]. The success of this database is clearly demonstrated by the increasing number of different research groups (see e.g. [19–37]) that make use of the data. The Amsterdam Light scattering setup was closed in 2007, but a modernized and improved descendant of the Dutch scattering apparatus, the IAA Cosmic Dust Laboratory (CoDuLab), has been constructed at the Instituto de Astrofísica de Andalucía (IAA) in Granada, Spain [38]. In the new apparatus the scattering angle range at which the measurements are performed is 3–177°. The measurements can be performed at five different wavelengths namely, 483, 488, 520, 568, and 647 nm. The first results of this instrument for water

* Corresponding author. Tel.: +34 958121311; fax: +34 958814530.
E-mail address: olga@iaa.es (O. Muñoz).

0022-4073/$ - see front matter © 2012 Elsevier Ltd. All rights reserved.
doi:10.1016/j.jqsrt.2012.01.014

droplets and for a sample of green clay particles, that had also been studied in Amsterdam, demonstrate the excellent performance of the Granadian instrument [39]. We proceed to make these data also available for the community in tabular form by constructing a new light scattering database, the Amsterdam–Granada Light Scattering Database (AGLSD), available at the website (www.iaa.es/scattering). This database consists of two branches, one with experimental data from Amsterdam and the other one with experimental data from Granada. By combining the data from the two instruments in one database we ensure the continued availability of the old data, and we prevent fragmentation of scattering data over different databases.

The purpose of this paper is to introduce the new Amsterdam–Granada Light Scattering Database, and to explain the improvements made to this database with respect to the old Amsterdam Light Scattering Database. The main improvements pertain to the user-friendliness of the database. By way of example we demonstrate the usefulness of the database by applying it to dust in the Martian atmosphere.

2. Amsterdam–Granada Light Scattering Database

In Fig. 1 we present the main page of the website of the Amsterdam–Granada Light Scattering Database (AGLSD). It consists of two branches from which experimental data from Amsterdam (Fig. 2) and Granada (Fig. 3) can be selected by clicking at the corresponding buttons. All measurements presented in the database have been previously published in peer-reviewed scientific journals predominantly in graphical form. References and access to the full text of those papers are also provided. Data in this database are freely available under the request of citation of this paper and the paper in which the used data were published. As in the Amsterdam branch, the heart of the AGLSD is the collection of tables and plots of the measured scattering matrix elements listed as functions of the scattering angle at different wavelengths. The database also includes information on the sample under study such as, size distribution, composition, origin, optical and/or scanning microscope images, and refractive indices of the particles. In addition, a detailed theoretical basis is provided to facilitate the correct use of the experimental data. Although the Amsterdam light scattering setup was closed in 2007 some of its experimental data have not been published yet. We update the AGLSD regularly with new data from Amsterdam and Granada. As shown in Fig. 1, new measurements included in the AGLSD will be highlighted in the main page as "Latest News". In this section we present the contents of the AGLSD, which hereafter will be referred to as the database.

2.1. Samples

The particle samples included in the database comprise a wide range in origin and composition, and have relevance for different subjects. Light scattering by particles with typical diameters (or volume-equivalent diameters) ranging from sub-micron to about 200 μm were

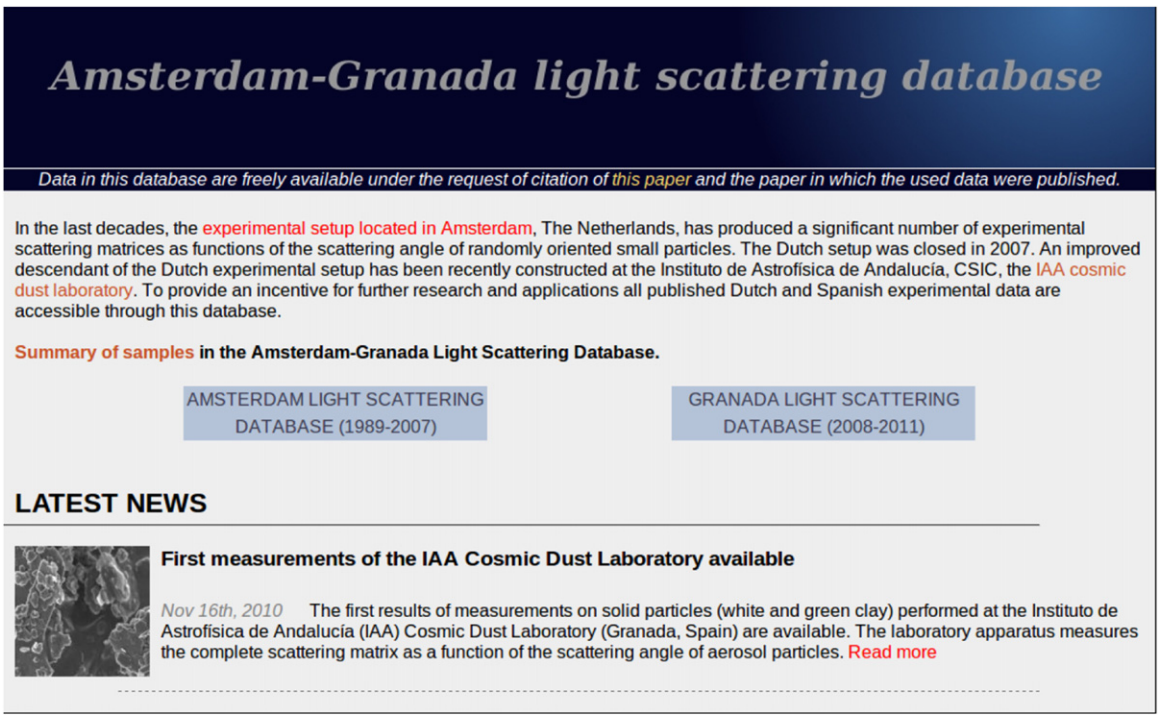

Fig. 1. Main page of the Amsterdam–Granada Light Scattering Database available at www.iaa.es/scattering.

Fig. 2. Amsterdam branch of Amsterdam–Granada Light Scattering Database.

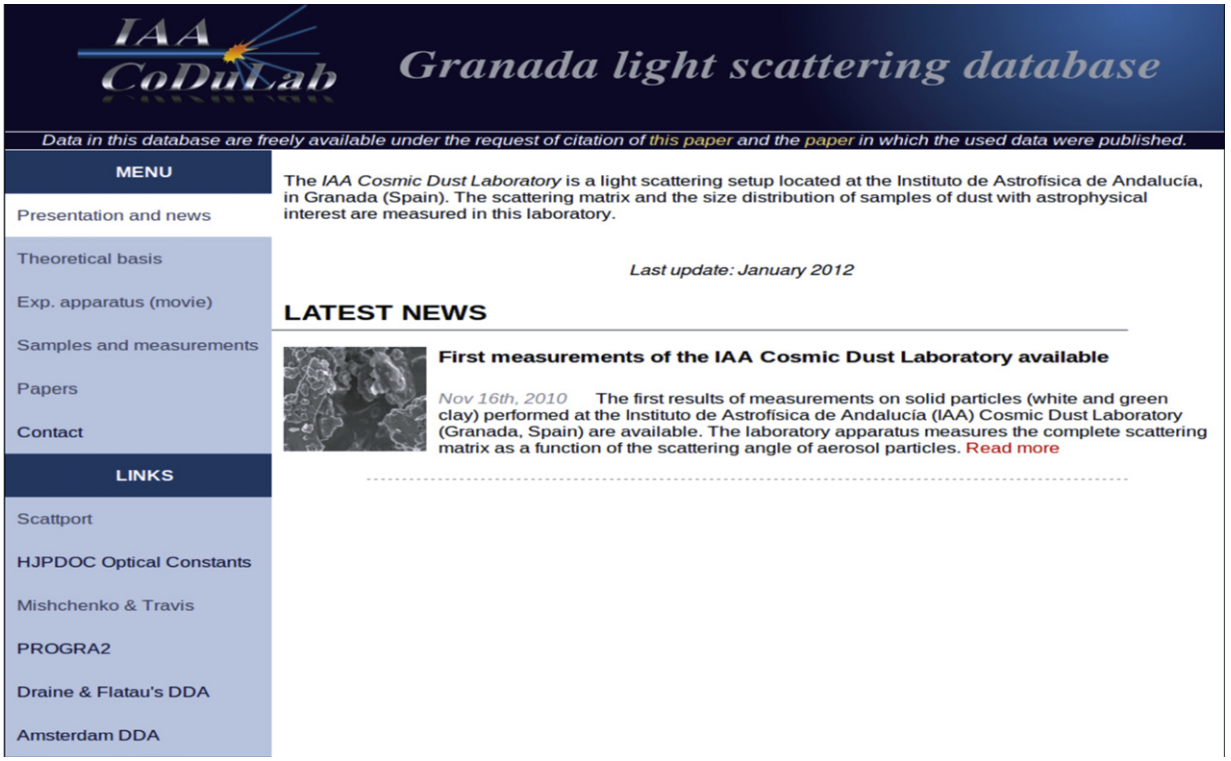

Fig. 3. Granada branch of Amsterdam–Granada Light Scattering Database.

measured with the experimental setups in Amsterdam and Granada. In Figs. 4 and 5, we present a complete table of samples included in the database at the time of writing this paper, together with some relevant information such as wavelengths, scattering angle range at which the measurements have been performed, and effective

Sample	r_{eff} (micron)	v_{eff}	Wavelengths (nm)	Angle range (deg.)
AEROSOLS				
Aggregates (fluffy) Sample 1	--	--	632.8	[5,174]
Aggregates (fluffy) Sample 2	--	--	632.8	[5,174]
Aggregates (fluffy) Sample 3	--	--	632.8	[5,174]
Aggregates (fluffy) Sample 4	--	--	632.8	[5,174]
Aggregates (fluffy) Sample 5	--	--	632.8	[5,174]
Aggregates (fluffy) Sample 6	--	--	632.8	[5,174]
Aggregates (fluffy) Sample 7	--	--	632.8	[5,174]
Allende Meteorite	0.8	3.3	632.8, 441.6	[5,173]
Clay Green (Amsterdam)	1.55	1.4	632.8, 441.6	[5,173]
Clay Green (Granada)	1.6	1.6	647	[3,177]
Clay Red	1.5	1.6	632.8, 441.6	[5,173]
Clay White	1.6	1.4	488, 647	[3,177]
Feldspar	1.0	1.0	632.8, 441.6	[5,173]
Fly Ash	3.65	10.9	632.8, 441.6	[5,173]
Forsterite Initial	1.8	5.4	632.8	[5,173]
Forsterite Small	1.3	3.1	632.8	[5,173]
Forsterite Washed	3.3	4.7	632.8	[5,173]
Hematite	0.4	0.6	632.8	[5,174]
Loess	3.9	2.6	632.8, 441.6	[5,173]
Martian Analog (palagonite)	4.5	7.3	632.8	[3,174]
Olivine L	3.8	3.7	632.8, 441.6	[5,173]
Olivine M	2.6	5.0	632.8, 441.6	[5,173]
Olivine S	1.3	1.8	632.8, 441.6	[5,173]
Olivine XL	6.3	6.8	632.8, 441.6	[5,173]
Quartz	2.3	2.3	632.8, 441.6	[5,173]
Rutile	0.13	0.5	632.8	[5,173]
Sahara Sand	8.2	4.0	632.8, 441.6	[5,173]
Sahara Sand (Libya)	124.75	0.15	632.8	[4,174]
Volcanic Ash (el chichon)	3.2	5.4	632.8	[5,173]
Volcanic Ash (Lokon)	7.1	2.6	632.8, 441.6	[5,173]
Volcanic Ash (Mount St. Helens)	4.1	9.5	632.8	[3,173]
Volcanic Ash (Pinatubo)	3.0	12.3	632.8, 441.6	[5,173]
Volcanic Ash (Redoubt A)	4.1	9.7	632.8	[3,173]
Volcanic Ash (Redoubt B)	6.4	7.6	632.8	[3,173]
Volcanic Ash (Spurr Anchorage)	4.8	8.8	632.8	[3,174]
Volcanic Ash (Spurr Ashton)	2.7	4.9	632.8	[3,174]
Volcanic Ash (Spurr Gunsight)	3.5	8.2	632.8	[3,174]
Volcanic Ash (Spurr stop 33)	14.4	6.6	632.8	[3,174]

Fig. 4. Summary of samples in the Amsterdam–Granada Light Scattering Database.

HYDROSOLS				
Anabaena flos aquae	3.09	0.012	632.8	[20,160]
Astrionella formosa	4.23	0.010	632.8	[20,160]
Emiliania huxleyi, no coccoliths	1.8	0.002	632.8	[35,145]
Emiliania huxleyi with coccoliths	1.8	0.07	632.8	[35,145]
Melosira granulata	3.74	0.004	632.8	[20,160]
Microcystis aeruginosa, no gas vacuoles	5.23	0.50	632.8	[20,160]
Microcystis aeruginosa with gas vacuoles	6.83	0.92	632.8	[20,160]
Microcystis sp.	1.87	0.063	632.8	[20,160]
Oscillatoria agardhii	1.64	0.044	632.8	[20,160]
Oscillatoria amoena	2.58	0.002	632.8	[20,160]
Phaeodactylum	16.4	0.23	632.8	[20,160]
Phaeocystis	12.2	0.43	632.8	[20,160]
Prochlorothrix hollandica	1.55	0.080	632.8	[20,160]
Selenastrum capricornutum	1.09	0.037	632.8	[20,160]
Volvox aureus	105	0.07	632.8	[20,160]
Westerschelde silt, 5-12 micron	5.93	0.00	632.8	[20,160]
Westerschelde silt, 3-5 micron	1.95	0.50	632.8	[20,160]
TEST PARTICLES				
Water Droplets	1.1	0.50	632.8, 441.6	[5, 173]
Water Droplets	rg=0.8 micron	sigmag=1.5	488, 520, 647	[3, 177]
AVERAGE AND SYNTHETIC SCATTERING MATRICES				
Average Aerosol Scattering Matrix	--	--	632.8 and 441.6 combined	[5,175]
Synthetic Average Volcanic Scattering Matrix	--	--	632.8	[0,180]
Synthetic Matrix Sahara Sand (Libya)	--	--	632.8	[0,180]
Synthetic Matrix Martian analog (palagonite) particles	--	--	632.8	[0,180]

Fig. 5. Continued from Fig. 4.

radii, r_{eff}, and variance, v_{eff}, as defined by Hansen and Travis [40]

$$r_{\text{eff}} = \frac{\int_0^\infty r\pi r^2 n(r)\,dr}{\int_0^\infty \pi r^2 n(r)\,dr} \tag{1}$$

$$v_{\text{eff}} = \frac{\int_0^\infty (r-r_{\text{eff}})^2 \pi r^2 n(r)\,dr}{r_{\text{eff}}^2 \int_0^\infty \pi r^2 n(r)\,dr} \tag{2}$$

where r is the radius and $n(r)$ is the size distribution of volume equivalent spheres. The values for r_{eff} and v_{eff}

presented in the complete table of samples are retrieved from the size distribution measurements based on the Fraunhofer diffraction theory (see Section 2.1.2). This table is available at the main page of the database under the "summary of samples" link (Fig. 1). Within the table, by clicking at the sample of interest the user is re-directed to the part of the database where the complete description of the sample and measurements are available. As shown in Figs. 4 and 5, a high percentage of the data presented in the database correspond to aerosol measurements although some measurements on hydrosols are also presented. Moreover, measurements on spherical water droplets that are used as test particles at different wavelengths are provided. For the water droplets measurements at 488, 520, and 647 nm we provide, instead of the effective radii and variance, the r_g and σ_g parameters corresponding to a log-normal size distribution as defined by Hansen and Travis [40].

2.1.1. General information

Once you are in any of the two branches by clicking on the name of a certain sample, general information concerning the sample is provided on a fact sheet. For instance, the origin of the sample is given together with qualitative estimates of its main constituents. They may give an indication of the refractive index of the bulk sample. For cases where the refractive index is not accurately known, we provide an estimate of the real part of the refractive index, Re(m), based on values found in the literature for the constituent minerals. Less information is usually available for the imaginary part of the refractive index, Im(m), because the natural variability within a mineral can be quite large. An indication of whether the value of Im(m) is relatively high or low is given by the color of the powdered sample, since white looking powders absorb little. The colors of the powders are mentioned or shown on photographs. For example, by clicking on the green clay sample you will see that its main constituent minerals are illite, kaolinite, montmorillonite, and quartz. Based on literature values [41–44], we may assume that the real part of the refractive index of green clay lies between 1.5 and 1.7, while the imaginary part likely lies in the range between 10^{-5} and 10^{-3} at visual wavelengths.

As mentioned, the scattering matrices of some of the samples presented in the database might be useful for various applications. As an example, clay particles are believed to occur on different Solar System bodies such as Mars, satellites, and asteroids. Clay is also an important component of mineral aerosols in the Earth atmosphere. This type of information will be provided for the new samples in the corresponding fact sheet under the *practical significance* item.

To give an indication of the shapes of the grains we provide one or more scanning electron microscope and/or optical images in the database for each sample. In order to check if the aerosol jet may change the shape/size of the particles during the measurements, either by breaking them up into smaller particles or by aggregating them into larger particles, we made several special test images. Field Emission Scanning Electron Microscope (FESEM) images were made for the sample under study as it was during the light scattering measurements, i.e. particles directly collected from the aerosol jet [39,45]. Comparison of images of the sample directly taken from the container and that taken from the jet stream showed no evidence of a significant alteration of the particles produced by the aerosol generator. This is illustrated in Fig. 6, which shows FESEM images of some green clay particles directly collected from the container (left panel) and from the aerosol jet stream (right panel). The FESEM/SEM images presented in the Granada branch (unless indicated otherwise) are taken from a glass slide briefly held in the aerosol jet at the place where it intersects with the laser beam.

It is important to note that the FESEM/SEM images in the database are not suited to infer detailed information about the sizes of the particles, mainly because they range over several orders of magnitude in most cases, so that images with lower magnification will be biased towards showing only larger particles, and vice versa.

Figures of the measured size distributions (Section 2.1.2) and scattering matrices (Section 2.2) are also provided, as well as the PDF file of the paper in which the data were published.

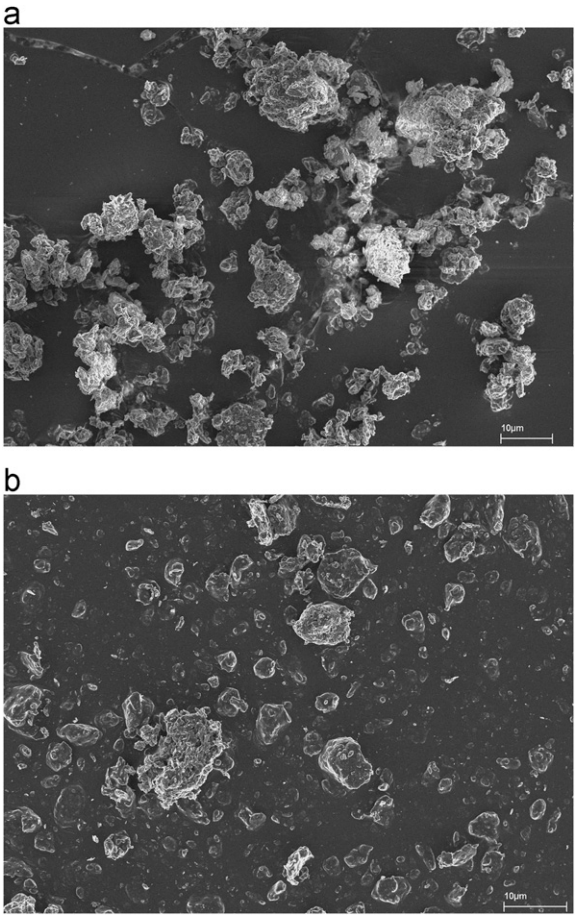

Fig. 6. FESEM images of green clay particles directly collected from the container (a) and collected from the aerosol jet (b).

2.1.2. Size distributions

Apart from shape and composition, size is a key property in determining the light scattering properties of small particles. In a collection of randomly oriented nonspherical particles we can replace each particle by a sphere with radius, r, having the same average (over all rotations) projected surface area or volume. In this way we can obtain size distributions. In the database we provide tables for normalized number, projected-surface-area, and volume size distributions. To plot these three size distributions in a convenient way a change of variables from r to $\log r$ is often performed, so that three different types of size distributions are formed, the normalized number distribution $N(\log r)$, the normalized projected-surface-area distribution $S(\log r)$, and the normalized volume distribution $V(\log r)$. In this way, equal areas under parts of the curve obtained by plotting $N(\log r)$ versus $\log r$, means equal relative number of particles per unit volume in the ranges considered. A similar property holds for plots of $S(\log r)$ and $V(\log r)$ versus $\log r$.

Size distributions as functions of radii, r, are common in the literature and often required for numerical applications. Thus, in addition to the mentioned $N(\log r)$, $S(\log r)$, and $V(\log r)$, the corresponding $n(r)$, $s(r)$, and $v(r)$ distributions for the new samples presented in the database will be also provided. Detailed information on how to transform one size distribution into another can be found in the database at www.iaa.es/scattering/site_media/sizedistributions.pdf and in [17]. It is often useful to characterize the sizes of the particles of a sample with two parameters: the effective radius r_{eff}, and effective standard variance v_{eff}. In the database we provide the calculated effective radius, r_{eff}, and the effective variance, v_{eff} as defined in [40] (see Eqs. (1) and (2)) for all our samples.

The projected-surface-area size distributions of the samples studied in Amsterdam were measured by using a Fritsch laser particle sizer [46] that employs the Fraunhofer diffraction theory for spheres. The particle sizer used in Granada is a Mastersizer 2000 from Malvern instruments. The Mastersizer measures the phase function of the sample at 633 nm in a certain scattering angle range with special attention to the forward scattering peak. Once it is measured it uses either Lorenz–Mie theory or Fraunhofer theory for spheres to retrieve the volume distribution that best fits the measured scattering pattern. It is clear that the retrievals from both methods are simplifications based on the assumption that the particles of the sample under study are spherical. Moreover, the Fraunhofer method has the restriction that the particles must be large compared to the wavelength of the incident light. However, at this moment this is the best that can be done as far as particle sizing for broad distributions of irregular particles is concerned. At the Granada branch we present the size distributions retrieved from both Fraunhofer and Lorenz–Mie theory so that the reader can choose which one is more appropriate for her/his purposes or take the average. As an example, Fig. 7 shows the measured $V(\log r)$ as a function of $\log r$ obtained from both, Fraunhofer and Lorenz–Mie theory for the green clay sample [4,39]. For comparison purposes we also present the $V(\log r)$ for a sample of Saharan dust collected in Libya (Sahara sand, Libya) [47]. In general, increasing the size of a particle with a certain shape promotes diffraction and the shapes of diffraction peaks of collections of randomly oriented particles are similar for different particle shapes as confirmed by various computations [48]. Thus, as shown in Fig. 7, results of both sizing methods tend to converge as the particles become larger, as is the case for the Sahara sand (Libya) sample that consists of particles larger than the wavelength of the incident light. In Table 1 we present the values of the effective radius, r_{eff}, and effective variance, v_{eff}, obtained from the measured size distributions in Amsterdam and Granada, respectively for the green clay and Sahara sand (Libya) samples. As shown, the values retrieved for r_{eff} and v_{eff} based on Fraunhofer theory in Amsterdam and Granada are very similar to each other even though the measurements have been performed far away in time ($\simeq$ 10 years) and with completely different devices.

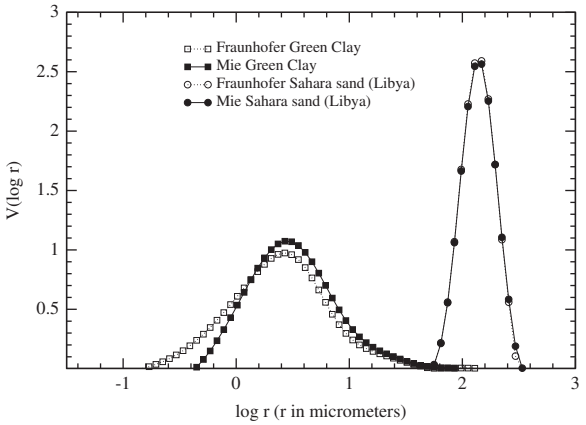

Fig. 7. Normalized volume distributions as a function of $\log r$ for the green clay and Sahara sand (Libya) samples. The volume distributions have been retrieved by assuming Lorenz–Mie (solid symbols) and Fraunhofer (empty symbols) theories.

Table 1
Effective radius and effective variance obtained from the measured size distributions of green clay and Sahara sand (Libya) in Amsterdam and Granada.

	Sample	Fraun. Ams	Fraun. Gr	Mie Gr
r_{eff}	Green clay	1.55 μm	1.62 μm	2.24 μm
v_{eff}	Green clay	1.40	1.57	1.08
r_{eff}	Sahara sand, Libya	124.75 μm	130.22 μm	130.90 μm
v_{eff}	Sahara sand, Libya	0.15	0.11	0.11

2.2. Measured scattering matrix elements

The flux and state of linear and circular polarization of a quasi-monochromatic beam of light can be described by means of the so-called flux vector whose elements are Stokes parameters [49,50]. If such a beam of light is singly scattered by an ensemble of particles and is observed from a distance much greater than the maximal linear dimension of the ensemble (far-field approximation [51]),

the flux vectors of the incident beam $\pi\mathbf{\Phi}_0$ and scattered beam $\pi\mathbf{\Phi}$ are, for each scattering direction, related by the so called 4×4 scattering matrix, $\mathbf{F}$, with elements F_{ij}. For randomly oriented particles, all scattering planes are equivalent. Thus, the scattering direction is fully described by the scattering angle θ, i.e. the angle between the directions of propagation of the incident and the scattered beams. Moreover, when randomly oriented irregular particles and their mirror particles are present in equal numbers in the ensemble, as is the case in our experiments, the scattering matrix has only six independent elements that are not identically equal to zero. A detailed description of the scattering matrix measured during the experiments can be found in the database at www.iaa.es/scattering/site_media/scatteringmatrix.pdf.

As mentioned, the measurements of our experimental apparatus must be performed under single scattering conditions. Therefore, we must have enough particles in the scattering volume to be representative for the ensemble of randomly oriented particles under study, but not so many that multiple scattering might start playing a role. Special test experiments were performed which show that our experimental results for scattering matrices are not significantly contaminated by multiple scattering [39,45].

It is important to remark that the measured values of $F_{11}(\theta)$ for the aerosol samples in the database are normalized so that they are equal to 1 at $\theta=30^\circ$ [5]. The function $F_{11}(\theta)$, normalized in this way, is proportional to the flux of the scattered light for unpolarized incident light and called the *phase function* or *scattering function* throughout the database. Furthermore, all scattering matrix elements, except $F_{11}(\theta)$ itself are given relative to $F_{11}(\theta)$, i.e., we present $F_{ij}(\theta)/F_{11}(\theta)$, with $i,j=1$–4 except for $i=j=1$. Also, for unpolarized incident light, the ratio $-F_{12}(\theta)/F_{11}(\theta)$ coincides with the *degree of linear polarization* of the scattered light. A detailed description of the scattering matrix elements tabulated in the database and the way they are normalized can be found in the database at www.iaa.es/scattering/site_media/normalization.pdf and in [18]. In addition to each measured matrix element (ratio) value, the experimental errors are also given. We refrain from listing the four element ratios $F_{13}(\theta)/F_{11}(\theta)$, $F_{14}(\theta)/F_{11}(\theta)$, $F_{23}(\theta)/F_{11}(\theta)$, and $F_{24}(\theta)/F_{11}(\theta)$, since we verified that these ratios never differ from zero by more than the experimental errors. This is consistent with scattering samples consisting of randomly oriented particles with equal amounts of particles and their mirror particles [49].

Different conventions are used for Stokes parameters and, in particular for the sign of the ratio of scattering matrix elements $F_{34}(\theta)/F_{11}(\theta)$. The convention employed here is in accordance with [49,50]. The scattering matrices given in the database satisfy the Cloude coherency matrix test as suggested by Hovenier et al. [50] within the accuracy of the measurements.

2.3. Average and synthetic matrices

The high similarity of the measured scattering matrices for different samples of irregular mineral compact particles induced us to construct an Average Aerosol Scattering matrix [5]. The Average is obtained from the measured scattering matrices of seven samples of irregular compact particles: feldspar, red clay, quartz, Pinatubo volcanic ash, loess, Lokon volcanic ash, and Sahara sand at two different wavelengths, 441.6 and 632.8 nm. The Average Aerosol Scattering Matrix is obtained as follows. First, the Average Aerosol phase function, $F_{11}(\theta)$, is determined by averaging the 14 phase functions measured at both wavelengths. Since no scattering cross-sections are available, the phase functions are averaged giving them equal weights. As mentioned in Section 2.2, the 14 measured phase functions are all normalized to one at 30° and this is also the case for the Average phase function. Second, each measured element ratio is multiplied by its corresponding normalized phase function, thus yielding elements instead of element ratios. Third, for each pair of indices (i,j) the elements $F_{ij}(\theta)$ of the Average Aerosol Scattering Matrix are obtained by averaging the 14 corresponding elements. Finally, division by the Average phase function yields the element ratios of the Average Aerosol Scattering Matrix. The resulting Average Matrix satisfies the Cloude test at each measured scattering angle.

A similar average scattering matrix was obtained for volcanic ash particles [6]. The average scattering matrices can be used, for example, in remote sensing studies for which the specific properties of the mineral aerosols or the volcanic ash are often not known (e.g. [11,16]). Moreover, using various computational techniques the average volcanic scattering matrix as well as the measured matrices for Sahara sand (Libya) [47], and the Martian analog (palagonite) particles [52] were extrapolated to cover the full range of scattering angles from 0° to 180° (e.g. [21,6]). These are called synthetic scattering matrices.

Tables of the Average Aerosol Scattering matrix and Synthetic Average Volcanic Scattering Matrix, as well as the mentioned synthetic scattering matrices for Sahara sand (Libya) and a Martian analog (palagonite) sample, are available in the database and can be directly accessible through the "summary of samples" table at the main page of the database (see Fig. 5).

3. Applications

The experimental data can be used in a direct manner, e.g. by comparison with astronomical observations of light scattered in single scattering conditions. Further, experimental scattering matrices are used to check the validity of advanced computational techniques devoted to simulate the scattering behavior of realistic polydisperse irregular particles e.g. [12,25,13,31,33,36,37,53–55]. Also the data can be used in an indirect manner if a method is applied to extrapolate the measured angular distributions of the scattering matrix elements to the full scattering angle range, including forward and backward scattering [21,47,56], the extrapolated functions can be used to perform multiple scattering calculations in scattering media such as planetary atmospheres and circumstellar disks of dust particles [9,21,10,53,19]. Apart from that, measuring all elements of the scattering matrix instead of one or two helps us in identifying errors in the electronics

or in the alignment of the optics involved in the experiment since all theoretical relationships valid for the elements of the scattering matrix [50,57] can be applied for tests.

3.1. An example: Martian atmosphere

Dust from the Martian surface is regularly swept up by winds and becomes suspended in the atmosphere of Mars. These airborne dust particles scatter and absorb solar radiation thereby playing a key role in determining the thermal structure of the thin Martian atmosphere. Thus, quantifying the effect of such particles in the atmosphere has been and still is a hot topic in Martian studies. This task is obviously far from trivial. This is not only due to the limitations of computational techniques to reproduce the scattering behavior of natural polydisperse irregular particles. In addition, astronomers have to face the lack of measurements of various input parameters needed for their radiative transfer codes (see e.g. [58–61], and references therein). The scattering function at a certain wavelength of Martian dust particles has been often derived by using the semi-empirical theory for nonspherical particles developed by Pollack and Cuzzi [62]. It is based on the use of Mie theory for spheres for the scattering function of particles smaller than a certain size parameter combined with results of approximate formulae for larger particles. Lately, the efforts have been focused on the use of more sophisticated model particles, namely cylinders, to calculate the phase function of Martian dust particles [61,63–66]. Even so, as pointed out by Wolff et al. [65], the calculated phase functions for a size distribution of cylinders produce a considerable overestimation of the phase function near backscattering direction when comparing with the Tomasko et al. [59] empirically derived phase functions of Martian dust. Therefore, the calculated phase functions require an empirical correction to remove the artificial backscattering enhancement that is not found either in the experimental phase functions for ensembles of randomly oriented irregular compact particles presented in the AGLSD (see e.g. Section 2.3).

As an example of the use of the AGLSD in Fig. 8, we show one of the four phase functions presented by Tomasko et al. [59] for Martian aerosols based on data of the Imager for Mars Pathfinder (IMP). In particular, we show the retrieved phase function at 671 nm corresponding to a gamma size distribution [40] with r_{eff} equal to 1.6 μm and v_{eff} equal to 0.2. In Fig. 8, we also present the experimental phase function for a palagonite sample [52] considered as a Martian dust analogue [67], the so called Martian analog (palagonite) sample. The palagonite sample has a real part of the refractive index, $\text{Re}(m)=1.5$ and an imaginary part, $\text{Im}(m)$, in the range 10^{-3} to 10^{-4} at visible wavelengths [68]. The r_{eff} and v_{eff} of the palagonite sample equal 4.5 μm and 7.3, respectively. The phase functions presented in Fig. 8 are normalized to unity at 30° scattering angle. Despite the differences in the size distributions of the Martian dust derived by Tomasko et al. [59] and the Martian analog (palagonite) sample, the agreement between both phase functions is remarkable.

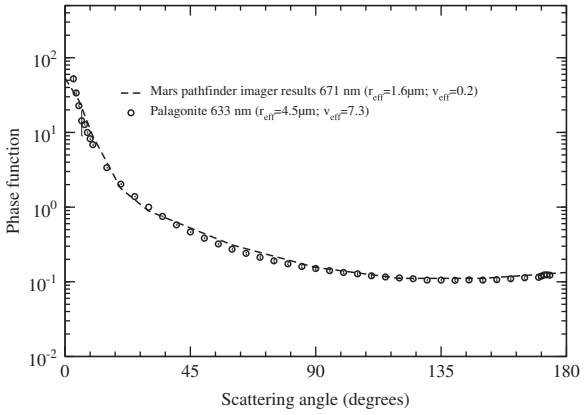

Fig. 8. Measured phase function of the Martian analog (palagonite) sample compared to the phase function derived by Tomasko et al. [59] for Martian dust particles. Both phase functions are normalized to 1 at 30° scattering angle.

The main discrepancies are related to the forward diffraction peak that is highly dependent on the size of the particles. This direct comparison suggests that the measured scattering function of the Martian analog (palagonite) sample may be considered a good approximation for Martian dust at the mentioned wavelengths.

4. Discussion and conclusion

A large collection of scattering matrices as functions of the scattering angle for irregular mineral particles is available in the Amsterdam–Granada Light Scattering Database. To ensure the reliability of these data only data that have been previously published in peer-reviewed scientific journals have been included in the AGLSD. To facilitate the correct use of the experimental data detailed theoretical information is also provided in the database e.g. on size distributions and scattering matrices. Data in this database are freely available under request of citation of this paper and the paper in which the used data were published. We plan to update this database regularly with new light scattering matrices for various samples of particles. We would appreciate to be informed about new works in which the experimental data presented in the AGLSD are used. That information would help us to obtain a realistic view on which samples are of major interest for the scientific community.

Acknowledgments

Timo Nousiainen and Michael Kahnert are heartily acknowledged for their encouragement and constructive suggestions on a previous version of the Amsterdam–Granada Light Scattering Database. Comments of M. Wolff and an anonymous referee on an earlier version of this paper are gratefully acknowledged. We are indebted to A. González from the Scientific Instrumentation Center of the University of Granada who took the FESEM images of the green clay sample. This work has been supported by the Plan Nacional

de Astronomía y Astrofísica under contract AYA2009-08190, and Junta de Andalucía, contract P09-FMQ-4555.

References

[1] Hovenier JW. Measuring scattering matrices of small particles at optical wavelengths. In: Mishchenko MI, Hovenier JW, Travis LD, editors. Light scattering by nonspherical particles. San Diego, CA: Academic; 2000. p. 355–65.

[2] Volten H, de Haan JF, Hovenier JW, Schreurs R, Vassen W, Dekker AG, et al. Laboratory measurements of angular distributions of light scattered by phytoplankton and silt. Limnol Oceanogr 1998;43:1180–97.

[3] Muñoz O, Volten H, de Haan JF, Vassen W, Hovenier JW. Experimental determination of scattering matrices of olivine and Allende meteorite particles. Astron Astrophys 2000;360:777–88.

[4] Muñoz O, Volten H, de Haan JF, Vassen W, Hovenier JW. Experimental determination of scattering matrices of randomly oriented fly ash and clay particles at 442 and 633 nm. J Geophys Res 2001;106:22833–44.

[5] Volten H, Muñoz O, Rol E, de Haan JF, Vassen V, Hovenier JW, et al. Scattering matrices of mineral aerosol particles at 441.6 nm and 632.8 nm. J Geophys Res 2001;106:17375–401.

[6] Muñoz O, Volten H, Hovenier JW, Veihelmann B, van der Zande WJ, Waters LBFM, et al. Scattering matrices of volcanic ash particles of Mount St, Helens, Redoubt, and Mount Spurr volcanoes. J Geophys Res 2004;109:D16201.

[7] Volten H, Muñoz O, Hovenier JW, Brucato JR, Colangeli L, Waters LBFM, et al. Scattering matrices and reflectance spectra of forsterite particles with different size distributions. J Quant Spectrosc Radiat Transfer 2006;100(1–3):429–36.

[8] Volten H, Muñoz O, Hovenier JW, Rietmeijer FJM, Nuth JA, Waters LBFM, et al. Experimental light scattering by fluffy aggregates of magnesiosilica, ferrosilica, and alumina cosmic dust analogs. Astron Astrophys 2007;470:377–86.

[9] Moreno F, Muñoz O, López-Moreno JJ, Molina A, Ortiz JL. A Monte Carlo code to compute energy fluxes in cometary nuclei. Icarus 2002;156(2):474–84.

[10] Mishchenko MI, Geogdzhayev IV, Liu L, Ogren JA, Lacis AA, Rossow WB, et al. Aerosol retrievals from AVHRR radiances: effects of particle nonsphericity and absorption and an updated long-term global climatology of aerosol properties. J Quant Spectrosc Radiat Transfer 2003;79/80:953–72.

[11] Herman M, Deuzé JL, Marchand A, Roger B, Lallart P. Aerosol remote sensing from POLDER/ADEOS over the ocean: improved retrieval using a nonspherical particle model. J Geophys Res 2005;110(D10) CiteID D10S02.

[12] Nousiainen T, Muinonen K, Raisanen P. Scattering of light by large Saharan dust particles in a modified ray optics approximation. J Geophys Res 2003;108(D1) AAC 12-1, CiteID 4025, doi:10.1029/2001JD001277.

[13] Dubovik O, Sinyuk A, Lapyonok T, Holben BN, Mishchenko M, Yang P, et al. Application of spheroid models to account for aerosol particle nonsphericity in remote sensing of desert dust. J Geophys Res 2006;111:D11208.

[14] Kahnert M, Rother T. Modeling optical properties of particles with small-scale surface roughness: combination of group theory with a perturbation approach. Opt Express 2011;19(12):11138–51.

[15] Garcia Muñoz A, Palle E, Zapatero Osorio MR, Martin EL. The impact of the Kasatochi eruption on the Moon's illumination during the August 2008 lunar eclipse. Geophys Res Lett 2011;38(14).

[16] Miffre A, Gregory D, Benjamin T, Rairoux P. Atmospheric non-spherical particles optical properties from UV-polarization lidar and scattering matrix. Geophys Res Lett 2011;38(16):1–7.

[17] Volten H, Muñoz O, Hovenier JW, de Haan JF, Vassen W, van der Zande WJ, et al. WWW scattering matrix database for small mineral particles at 441.6 and 632.8 nm. J Quant Spectrosc Radiat Transfer 2005;90(2):191–206.

[18] Volten H, Muñoz O, Hovenier JW, Waters LBFM. An update of the Amsterdam Light Scattering Database. J Quant Spectrosc Radiat Transfer 2006;100:437–43.

[19] Braak CJ, de Haan JF, van der Mee CVM, Hovenier JW, Travis LD. Parametrized scattering matrices for small particles in planetary atmospheres. J Quant Spectrosc Radiat Transfer 2001;69:585–604.

[20] Mishchenko MI, Travis LD, Lacis AA. Scattering, absorption, and emission of light by small particles. Cambridge: Cambridge University Press; 2002.

[21] Liu L, Mishchenko MI, Hovenier JW, Volten H, Muñoz O. Scattering matrix of quartz aerosols: comparison and synthesis of laboratory and Lorenz Mie results. J Quant Spectrosc Radiat Transfer 2003; 79/80:911–20.

[22] Zubko E, Shkuratov Y, Hart M, Eversole J, Videen G. Backscattering and negative polarization of agglomerate particles. Opt Lett 2003;28(17):1504–6.

[23] Vilaplana R, Moreno F, Molina A. Computations of the single scattering properties of an ensemble of compact and inhomogeneous rectangular prisms: implications for cometary dust. J Quant Spectrosc Radiat Transfer 2004;88:219–31.

[24] Veihelmann B, Nousiainen T, Kahnert M, van der Zande WJ. Light scattering by small feldspar particles simulated using the Gaussian random sphere. J Quant Spectrosc Radiat Transfer 2006;100: 393–405.

[25] Min M, Hovenier JW, de Koter A. Modeling optical properties of cosmic dust grains using a distribution of hollow spheres. Astron Astrophys 2005;432(3):909–20.

[26] Rosenbush V, Kiselev N. Polarization opposition effect for the Galilean satellites of Jupiter. Icarus 2005;179(2):490–6.

[27] Kahnert M, Nousiainen T. Uncertainties in measured and modeled asymmetry parameters of mineral dust. J Quant Spectrosc Radiat Transfer 2006;100:173–8.

[28] Nousiainen T, Kahnert M, Veihelmann B. Light scattering modeling of small feldspar aerosol particles using polyhedral prisms and spheroids. J Quant Spectrosc Radiat Transfer 2006;101(3): 471–87.

[29] Tafuro AM, Barnaba F, de Tomasi F, Perrone MR, Gobbi GP. Saharan dust particle properties over the central Mediterranean. Atmos Res 2006;81(1):67–93.

[30] Kahnert M, Nousiainen T, Räisänen P. Mie simulations as an error source in mineral aerosol radiative forcing calculations. Q J R Meteorol Soc 2007;133:299–307.

[31] Moreno F, Muñoz O, Guirado D, Vilaplana R. Comet dust as a size distribution of irregularly shaped compact particles. J Quant Spectrosc Radiat Transfer 2007;106:348–59.

[32] Cloude SR. Depolarization by aerosols: entropy of the Amsterdam Light Scattering Database. J Quant Spectrosc Radiat Transfer 2009;110:1665–76.

[33] Muinonen K, Nousiainen T, Lindqvist H, Muñoz O, Videen G. Light scattering by Gaussian particles with internal inclusions and roughened surfaces using ray optics. J Quant Spectrosc Radiat Transfer 2009;110:23.

[34] Meng Z, Yang P, Kattawar GW, Bi L, Liou KN, Laszlo I. Single-scattering properties of tri-axial mineral dust aerosols: a database for application to radiative transfer calculations. J Aerosol Sci 2010;41:501–12.

[35] Tyynelä J, Zubko E, Muinonen K, Videen K. Interpretation of single-particle negative polarization at intermediate scattering angles. Appl Opt 2010;49(28):5284–96.

[36] Bi L, Yang P, Kattawar GW, Kahn R. Modeling optical properties of mineral aerosol particles by using nonsymmetric hexahedra. Appl Opt 2010;49(3):334–41.

[37] Ishimoto H, Zaizen Y, Uchiyama A, Masuda K, Mano Y. Shape modeling of mineral dust particles for light-scattering calculations using the spatial Poisson-Voronoi tessellation. J Quant Spectrosc Radiat Transfer 2010;11:2434–43.

[38] Muñoz O, Moreno F, Guirado D, Ramos JL, López A, Girela F, et al. The new IAA light scattering apparatus. J Quant Spectrosc Radiat Transfer 2010;111:187–96.

[39] Muñoz O, Moreno F, Guirado D, Ramos JL, Volten H, Hovenier JW. The IAA cosmic dust laboratory: experimental scattering matrices of clay particles. Icarus 2011;211(1):894–900.

[40] Hansen JE, Travis LD. Light scattering in planetary atmospheres. Space Sci Rev 1974;16:527–610.

[41] Kerr PF. Optical mineralogy. New York: McGraw-Hill; 1959.

[42] Egan WG, Hilgeman TW. Optical properties of inhomogeneous materials: applications to geology, astronomy, chemistry, and engineering. San Diego, CA: Academic; 1979.

[43] Gerber HE, Hindman EE, editors. Light absorption by aerosol particles. In: Technical proceedings of the first international workshop on light absorption by aerosol particles, Fort Collins, Colorado, 1980. Hampton, VA: Spectrum; 1982.

[44] Klein C, Hurlbut Jr CS. Manual of mineralogy. New York: John Wiley; 1993.

[45] Hovenier JW, Volten H, Muñoz O, van der Zande WJ, Waters LBFM. Laboratory studies of scattering matrices for randomly oriented particles: potentials, problems and perspectives. J Quant Spectrosc Radiat Transfer 2003;79–80:741–55.

[46] Konert M, Vandenberghe J. Comparison of laser grain size analysis with pipette and sieve analysis: a solution for the underestimation of the clay fraction. Sedimentology 1997;44:532–5.
[47] Muñoz O, Volten H, Hovenier JW, Nousiainen T, Muinonen K, Guirado D, et al. Scattering matrix of large Saharan dust particles: experiments and computations. J Geophys Res 2007;112: D13215, doi:10.1029/2006JD008074.
[48] Mishchenko MI. Electromagnetic scattering by nonspherical particles. A tutorial review. J Quant Spectrosc Radiat Transfer 2009;110(11): 802–32.
[49] van de Hulst HC. Light scattering by small particles. NY: John Wiley & Sons Inc.; 1959 Also Dover Publications Inc. N.Y., 1981.
[50] Hovenier JW, van der Mee CVM, Domke H. Transfer of polarized light in planetary atmospheres: basic concepts and practical methods. Dordrecht: Kluwer/Springer; 2004.
[51] Mishchenko MI, Hovenier JW, Mackowski DW. Single scattering by a small volume element. J Opt Soc Am A 2004;21(1):71–87.
[52] Laan EC, Volten H, Stam DM, Muñoz O, Hovenier JW, Roush TL. Scattering matrices and expansion coefficients of martian analogue palagonite particles. Icarus 2009;199:219–30.
[53] Veihelmann B, Volten H, van der Zande WJ. Simulations of light reflected by an atmosphere containing irregular shapes mineral aerosol over the ocean. Geophys Res Lett 2004, doi:0.1029/2003GL018229.
[54] Nousiainen T, Vermeulen K. Comparison of measured single-scattering matrix of feldspar particles with T-matrix simulations using spheroids. J Quant Spectrosc Radiat Transfer 2003;79–80:1031–42.
[55] Nousiainen T, Muñoz O, Lindqvist H, Mauno P, Videen G. Light scattering by large Saharan dust particles: comparison of modeling and experimental data for two samples. J Quant Spectrosc Radiat Transfer 2010, doi:10.1016/j.jqsrt2010.09.003.
[56] Kahnert M, Nousiainen T. Variational data-analysis method for combining laboratory-measured light-scattering phase functions and forward-scattering computations. J Quant Spectrosc Radiat Transfer 2007;103:27–42.
[57] Hovenier JW, van der Mee CVM. Testing scattering matrices, a compendium of recipes. J Quant Spectrosc Radiat Transfer 1996;55: 649–61.
[58] Markiewicz WJ, Sablotny RM, Keller HU, Thomas N. J Geophys Res 1999;104:9009–17.
[59] Tomasko MG, Doose LR, Lemmon M, Smith PH, Wegryn E. Properties of dust in the Martian atmosphere from the imager on Mars pathfinder. J Geophys Res 1999;104:8987–9007.
[60] Banfield JL. Global mineral distributions on Mars. J Geophys Res 2002;107:23, doi:10.1029/2001JE001510.
[61] Wolff MJ, Smith MD, Clancy RT, Spanovich N, Whitney BA, Lemmon MT, et al. Constraints on dust aerosols form the Mars exploration rovers using MGS overflights and Mini-Tes. J Geophys Res 2006;111:E12S17, doi:10.1029/2006JE002786.
[62] Pollack JB, Cuzzi JN. Scattering by nonspherical particles of size comparable to a wavelength: a new semi-empirical theory and its application to tropospheric aerosols. J Atmos Sci 1980;37:868–81.
[63] Wolff MJ, Smith MD, Clancy RT, Arvidson R, Kahre M, Seels IV F, et al. Wavelength dependence of dust aerosol single scattering albedo as observed by the Compact Reconnaissance Imaging Spectrometer. J Geophys Res 2009;114 doi:10.1029/2009JE003350.
[64] Vincendon M, Langevin Y, Poulet F, Pommerol A, Wolff M, Bibring J-P, et al. Yearly and seasonal variations of low albedo surfaces on Mars in the OMEGA/MEx dataset: constraints on aerosol properties and dust deposits. Icarus 2009;200:395–405.
[65] Wolff MJ, Clancy RT, Goguen JD, Malin MC, Cantor BA. Ultraviolet dust aerosol properties as observed by MARCI. Icarus 2010;208: 143–55.
[66] Madeleine J-B, Forget F, Millour E, Montabone L, Wolff MJ. Revisiting the radiative impact of dust on Mars using the LMD Global Climate Model. J Geophys Res 2011;116 doi:10.1029/2011JE003855.
[67] Roush TL, Bell JF. Thermal emission measurements 2000-400/cm (525 micrometers) of Hawaiian palagonitic soils and their implications for Mars. J Geophys Res 2005;100:5309–17.
[68] Clancy RT, Lee SW, Gladstone GR, McMillan WW, Roush T. A new model for Mars atmospheric dust base upon analysis of ultraviolet through infrared observations from Mariner 9, Viking, and Phobos. J Geophys Res 1995;100:5251–63.